Clays and Clay Minerals, Vol. 39, No. 1, 54–69, 1991.

DIAGENETIC STRUCTURAL TRANSFORMATIONS IN NORTH SEA JURASSIC ILLITE/SMECTITE

HOLGER LINDGREEN,[1] HANS JACOBSEN,[2] AND HANS JØRGEN JAKOBSEN[2]

[1] Institute of Mineralogy, University of Copenhagen
Øster Voldgade 10, DK-1350 Copenhagen K, Denmark

[2] Department of Chemistry, University of Aarhus
DK-8000 Aarhus C, Denmark

Abstract—The Kimmeridgian-Volgian(-Ryazanian) claystone is the principal oil source rock in the troughs of the North Sea. Randomly (R0) ordered mixed-layer illite/smectite (I/S) appears to have transformed to R1-(IS) or R3-(ISII) ordered simultaneously with oil generation. The proportion of illite layers in I/S increased to 95% during diagenesis in these claystones. Exceptions are three samples of I/S of probably bentonitic origin; these have apparently changed during diagenesis to R0-ordered I/S containing 40–50% illite layers. Fine fractions of the claystones dominated by I/S were analyzed by ^{27}Al and ^{29}Si magic-angle spinning (MAS)-nuclear magnetic resonance (NMR) spectroscopy, ^{57}Fe Mössbauer spectroscopy, and X-ray powder diffraction (XRD), and for total chemical composition. Si/Al ratios determined from MAS-NMR agree closely with those calculated from total chemical analysis; however, tetrahedral and octahedral Al occupancies were most accurately determined by NMR. An increase in the percentage of illite layers and in the ordering of the I/S was accompanied by fixation of K^+ and NH_4^+ in the I/S, by tetrahedral Al-for-Si substitution, and by octahedral Al-for-(Mg + Fe) substitution, resulting both in an increase of charge in the 2:1 layers and in a migration of charge from octahedral to tetrahedral sheets. The I/S of probably bentonitic origin had a larger tetrahedral and a smaller octahedral charge than expected from its content of illite layers. MAS-NMR showed a significantly higher content of tetrahedral Al (most likely in smectitic sites) than expected from the percentage of illite layers calculated from XRD. Correspondingly, XRD of K^+-saturated and glycolated specimens showed that several smectite layers possessed a significant charge. A constant *b*-dimension of the I/S and the presence of a significant charge in the smectite layers suggest that a transformation of smectite to illite layers in the I/S by tetrahedral Al-for-Si substitution followed by interlayer cation fixation and interlayer contraction is the most probable genesis for the I/S investigated.

Key Words—Chemical composition, Diagenesis, Illite/smectite, Mössbauer spectroscopy, Nuclear magnetic resonance, X-ray powder diffraction.

INTRODUCTION

Smectite layers in mixed-layer illite/smectite (I/S) are converted to illite layers during burial diagenesis (Perry and Hower, 1972). Smectite layers contain as much as 0.6 negative charge per $O_{10}(OH)_2$ unit, vermiculite layers from 0.6 to 0.9, and mica layers about 1.0 (Bailey, 1984). Thus, a net increase in negative charge is necessary for the formation of an illite layer from a smectite layer. From Mössbauer spectroscopic data on smectites from the disturbed belt of Montana, Eslinger *et al.* (1979) indicated that as much as 30% of the total charge increase in I/S occurs in the octahedral sheet through Fe-reduction during metamorphism. Most of the charge increase during illite layer formation, however, occurs by Al^{3+}-for-Si^{4+} substitution in the tetrahedral sheet (Foscolos *et al.*, 1976; Eberl and Hower, 1976; Eslinger *et al.*, 1979; Hower, 1981). The reaction mechanism for this charge increase has been discussed in several papers. Investigation of diagenetic clays (Hower *et al.*, 1976) and hydrothermal experiments (Eberl, 1976; Eberl and Hower, 1976) indicate a transformation in which Al^{3+} substitutes for Si^{4+} in the tetrahedral sheet, followed by interlayer potassium fixation and interlayer contraction. On the other hand, combined X-ray powder diffraction (XRD) and transmission electron microscopy (TEM) studies of dispersed illitic clays from bentonites and sandstones led Nadeau *et al.* (1985) to propose a neoformation mechanism, i.e., a dissolution of smectite and precipitation/growth of thin illite particles.

So far, the structural transformations have been discussed on the basis of data from XRD, scanning electron microscopy, microprobe analysis, and chemical analysis, supplemented in one study of mixed-layers by Mössbauer spectroscopy (Eslinger *et al.*, 1979) and in one study by ^{29}Si MAS-NMR (Altaner *et al.*, 1988). Using XRD and ^{29}Si MAS-NMR, Altaner *et al.* (1988) investigated samples of I/S containing 90–100% illite layers and one rectorite containing 50% illite layers. The percentage of smectite layers calculated from ^{29}Si NMR data was significantly higher than the percentage obtained from XRD data. They concluded that tetrahedral sheets having minor Al-for-Si substitution (the

Copyright © 1991, The Clay Minerals Society

https://doi.org/10.1346/CCMN.1991.0390108 Published online by Cambridge University Press

typical smectite substitution pattern) must be present in the illite particles. Therefore, these particles were most likely formed by Al-for-Si replacement, the mechanism proposed by Hower *et al.* (1976), and not by a neoformation and growth of illite particles, the mechanism proposed by Nadeau *et al.* (1985).

In recent years, the technique of high-resolution MAS-NMR spectroscopy (^{27}Al and ^{29}Si) of solids has grown into an increasingly important tool in studies of synthetic and natural clay minerals (Goodman and Stucki, 1984; Thompson, 1984; Kinsey *et al.*, 1985; Komarnemi *et al.*, 1986; Weiss *et al.*, 1987; Altaner *et al.*, 1988; Jakobsen *et al.*, 1988b). In a preliminary report Jakobsen *et al.* (1988b) showed that ^{27}Al and ^{29}Si MAS-NMR, especially at high spinning speeds, may be used successfully to determine the Al^{IV}/Al^{VI} and Si/Al^{IV} ratios in natural clays. Together, $^{27}Al/^{29}Si$ MAS-NMR and ^{57}Fe Mössbauer spectroscopies can be used as non-destructive methods to obtain information about the distribution within the intact I/S of the major elements, except for Mg and the interlayer cations.

Upper Jurassic claystone of Kimmeridgian-Volgian(-Ryazanian) age is the main source rock for oil in the Central Trough, North Sea (Barnard and Cooper, 1981). The ordering and increase in the percentage of illite in I/S from the North Sea and onshore Denmark have previously been investigated by XRD on dispersed I/S and by high-resolution transmission electron microscopy (HRTEM) on intact rock (Hansen and Lindgreen, 1989). These results indicate that the randomly (R0) ordered I/S containing ~70% illite layers is mainly detrital. It becomes ordered during diagenesis, and the proportion of illite layers increases to ~90%. Three of the samples examined in the present study, from well 2/7-3 (from a depth of 3365 m and 3502 m) and from well W1 (3816 m depth) probably came, according to Hansen and Lindgreen (1989), from bentonites formed from volcanic ash and probably changed during diagenesis into R0-ordered I/S containing 40–50% illite layers.

The aim of the present study was to correlate the percentage of illite layers in I/S and the degree of ordering in I/S with I/S chemical composition determined by ^{27}Al and ^{29}Si MAS-NMR, by Mössbauer spectroscopy, and by chemical analysis. These results were further used to elucidate the elemental and structural changes in the I/S during the transformation of smectite to illite layers through burial diagenesis in the North Sea. These changes are discussed in relation to the solid-state transformation and the neoformation models of illite genesis.

MATERIALS AND METHODS

Materials

Materials from the Mandal, Farsund, and Haugesund Formations in the Central Trough, North Sea (Figure 1), were collected as cuttings from the Danish wells E1, G1, I1, M8, U1, W1, Adda 1, and Lulu 1 and the Norwegian wells 2/7-3 and 2/11-1 and as core material from wells E1 and 2/11-1.

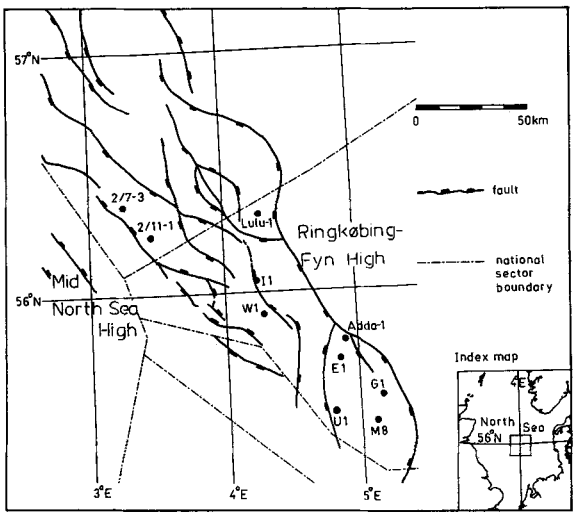


Figure 1. Location map of wells for North Sea illite/smectite samples.

Nomenclature

The symbols I and S are used to represent illite and smectite layers, respectively. In the present work the fraction of illite layers in I/S is presented by the symbol P_I, i.e., the probability of finding an illite layer in the mixed-layer. $P_{S,I}$ is the probability that an illite layer succeeds a smectite layer, $P_{SI,I}$ is the probability that an illite layer succeeds an SI unit, and $P_{SII,I}$ is the probability that an illite layer succeeds an SII unit. The ordering values used are R0 for random ordering, R1 for rectorite ordering, and R3 for Kalkberg ordering (Reynolds, 1984). Al^{IV} and Al^{VI} are used as symbols for tetrahedrally and octahedrally coordinated Al, respectively.

Sample preparation

All cuttings were washed in distilled water and dried at room temperature. Dark-grey rock fragments, typical of the formations studied and dominating the sample intervals, were selected for analysis.

The samples were treated with NaOAc at pH 5.5 and 100°C to remove calcite, followed by Na hypochlorite treatment at pH 9.0 and 100°C to remove organic matter (Anderson, 1963), and finally by Na dithionite, Na bicarbonate, and Na citrate at pH 7 to remove iron and aluminum oxides and oxyhydroxides (Roth *et al.*, 1969). About 100 mg of dithionite was used per gram of sample. Preliminary experiments with a glauconite sample showed that these treatments did not produce changes in the Mössbauer spectrum of this mineral. The sand and silt fractions were then removed by conventional centrifugation or by elutriation (Jensen and Hansen, 1961), and the fine (<0.2-μm) and coarse (0.2–2.0-μm) clay fractions were separated in a continuous flow centrifuge. I/S was isolated from the fine-clay fraction by the ethanol-water procedure (Buzagh and Szepesi, 1955) used previously for the separation of montmorillonite (Gibbs, 1967). By this procedure discrete illite and kaolinite, present in fair amounts (>10%) even in the fine-clay fraction, were largely removed from the Central Trough samples. NH_4^+ was not added to the samples at any step during preparation, except for the NH_4^+-saturated portions of the fine-clay fractions used in total chemical analysis (see below).

https://doi.org/10.1346/CCMN.1991.0390108 Published online by Cambridge University Press

X-ray powder diffraction

Specimens were prepared for X-ray powder diffraction (XRD) by the pipet method using 2.5 mg of sample per square centimeter. Tests using other sample densities showed this density to be infinitely thick to the radiation applied in the range 0°–25°2θ. XRD was carried out using CrKα and CuKα radiation and a Philips goniometer PW 1771/00 with a 2θ variable divergence slit and a monochromator. For each sample, a series of K^+-, Mg^{2+}-, and Na^+-saturated air-dried specimens was prepared. After XRD analysis, the specimens were glycolated at 60°C for 3 days (further glycolation for as long as 9 days did not change the diffractograms) and again analyzed by XRD. Finally, a K^+-saturated air-dried specimen of each sample was heated for 1 hr at 250°C before XRD analysis.

The diffractograms of the Mg^{2+}-saturated air-dried and the K^+-saturated glycolated specimens were simulated using the NEWMOD computer program for two-component mixed-layering (Reynolds, 1984; Bethke and Reynolds, 1986). Diffractograms of the Mg^{2+}-saturated glycolated specimens were simulated using both the NEWMOD program and a program reported by Cradwick and Wilson (1978) for three-component mixed-layering. The quality of the simulations was evaluated from peak positions, peak heights, and peak shapes (the criteria of Reynolds, 1984), in our diffractograms between 6° and 30°2θ.

^{27}Al and ^{29}Si MAS-NMR spectroscopy

^{27}Al and ^{29}Si MAS-NMR spectra were obtained using a Varian XL-300 spectrometer (7.1 T) at 78.16 and 59.59 MHz, respectively. For a few samples, spectra were also recorded on Varian VXR-400S (9.4 T) and VXR-500 (11.7 T) spectrometers for comparison of the quadrupolar coupling parameters and chemical shift data determined at the lower (7.1 T) magnetic field strength. All spectrometers employed home-built high-speed spinning MAS probes of double air-bearing design (Jakobsen *et al.*, 1988a) for 7 mm o.d. (220-μl sample volume) or 5 mm o.d. cylindrical rotors (130-μl sample volume) with a maximum spinning speed of 10 and 16 kHz, respectively. These high spinning speeds ensured efficient suppression of dipolar interactions with abundant spin I = ½ nuclei (^{1}H) and paramagnetic sites or ions. Furthermore, the intensities of interfering spinning sidebands for the central ^{27}Al transition were reduced and the quality of the experimental spectra greatly improved (Jakobsen *et al.*, 1988a). Zirconia (PSZ-700 HP) 7-mm rotors and a spinning speed of 7.2 kHz were used for ^{29}Si observation and Si_3N_4 7-mm rotors with a speed of 9–10 kHz for the ^{27}Al MAS experiments. For selected samples, ^{27}Al MAS spectra were recorded using a spinning speed of 13.5 kHz in 5-mm Si_3N_4 rotors. The magic angle was set by observing the rotational echoes in the FID of the ^{79}Br resonance for KBr (Frye and Maciel, 1982) in a dynamic mode. For the ^{27}Al MAS experiments, the magic angle was checked and set accurately in the same manner using the ^{27}Al resonance for a sample of hydrated calcium aluminate cement ($Ca_3Al_2O_6 \cdot 6D_2O$; Jakobsen *et al.*, 1988a). To ensure quantitatively correct determination of the Al^{IV}/Al^{VI} ratios short radiofrequency pulses of 1.5 μs ($\sim\pi/4$ solid pulse) and a relaxation delay of 1.0 s were employed for ^{27}Al. For the ^{29}Si MAS spectra, 3.0-μs pulses ($\sim\pi/5$ pulses) and a relaxation delay of 8.0 s were used. The spectral intensities for the individual resonances in both the ^{27}Al and ^{29}Si MAS spectra were determined by deconvolution using the computer program SIMULL as by Jakobsen *et al.* (1988b). The Al^{IV}/Al^{VI} ratios were obtained directly from the deconvoluted Al^{IV} and Al^{VI} intensities. Si/Al^{IV} ratios were calculated from the intensities of the Si(nAl) (n = 0, 1, 2) resonances determined from the deconvoluted ^{29}Si MAS spectra according to the equation

$$Si/Al^{IV} = \sum_{n=0}^{3} I_{Si(nAl)} / \sum_{n=0}^{3} (n/3) I_{Si(nAl)} . \quad (1)$$

This equation is related to that used for calculating Si/Al ratios of framework zeolites (Thomas and Klinowski, 1985). ^{27}Al and ^{29}Si chemical shifts (ppm) were referenced to external samples of 1.0 M $AlCl_3 \cdot 6H_2O$ in H_2O and tetramethylsilane, respectively. The $^{27}Al^{IV}$ and $^{27}Al^{VI}$ chemical shifts were corrected for the second-order quadrupolar shifts for the two resonances. Second-order quadrupolar shifts were determined from the shift of the observed spinning sideband positions for the satellite transitions relative to the center of gravity for the centerband using the procedure described recently (Samoson, 1985) and employed for other clay samples (Jakobsen *et al.*, 1988b). This procedure also gave values for the second order quadrupolar effect (SOQE) parameters, i.e., the product $(QCC)(1 + \eta^2/3)^{1/2}$ where QCC and η are the quadrupolar coupling constant and asymmetry parameter, respectively, for the clay samples studied.

Mössbauer spectroscopy

Mössbauer spectra were obtained using a constant acceleration spectrometer and a source of ^{57}Co in Pd. Isomer shifts are given relatively to the centroid of the spectrum of α-Fe at room temperature. Analyses were performed on selected Na^+-saturated I/S samples at room and liquid nitrogen temperature and with the absorber plane normal to or at an angle of 54.7° to the radiation. Spectra were computerfitted by Lorentzian lineshapes; the widths and areas of the two component peaks in each quadrupole doublet were constrained to be equal.

Infrared spectroscopy

Analysis by infrared spectroscopy (IR) was carried out on a Bruker 113V Fourier spectrometer. KBr pellets with 0.3-mg sample were heated for 16 hr at 140°C and analyzed.

Total chemical analysis

Total chemical analysis was made using the $HF\text{-}H_3BO_3$ dissolution procedure in Teflon bombs (Bernas, 1968), followed by atomic absorption spectrophotometric determination of dissolved Na, Mg, Ca, Fe, Al, and Si. Prior to the dissolution the purified mixed-layer samples were Na^+-saturated and air-dried. Portions (50 mg) of the NH_4^+-saturated samples were also analyzed. The oxide composition was calculated as a percentage of the sum of the oxides.

NH_4^+ was determined by an isotope dilution method (Middelboe, 1977). NH_4^+-nitrogen was released as NH_3 and oxidized to N_2 by heating small samples (about 1 mg) with CuO and a known amount of $^{15}NH_4Cl$ in evacuated glass ampuls for at least 3 hr at 600°C. Prolonged heating or higher heating temperatures did not increase the amount of NH_3 released. The relative amounts of ^{15}N and ^{14}N were then determined by optical emission spectroscopy, and the N-content in the sample was calculated from the $^{14}N/^{15}N$ ratio.

RESULTS

X-ray powder diffraction

The probabilities obtained by the simulations of the diffractograms of Mg^{2+}-saturated and air-dried specimens and Mg^{2+}-saturated and glycolated specimens agree within 0.05 P_1-units for each sample. Thus, only the results for the glycolated specimens are given in

https://doi.org/10.1346/CCMN.1991.0390108 Published online by Cambridge University Press

Table 1. Results of X-ray powder diffraction (CuKα) analysis of illite/smectite samples from the North Sea.

Well depth (m)	Mg^{2+}-saturated specimens (air-dry and glycolated) P_I	$P_{S.I}$	$P_{SI.I}$	$P_{SII.I}$	Reich-weite	K^+-saturated specimens (glycolated) P_I	$P_{S.I}$
E1							
2983[co]	0.65	0.45	0.76	0.76	R0	0.82	0.82
3444[cu]	0.80	1.00	0.55	0.82	R1		
3828[cu]	0.80	1.00	0.45	0.85	R1	0.95	0.95
3938[cu]	0.85	1.00	0.55	0.88	R1	0.85	0.85
G1							
2609[cu]	0.75	0.65	0.78	0.78	R0		
3441[cu]	0.70	3-component (0.10 vermiculite, 0.20 smectite)					0.85
M8							
2368[cu]	0.65	0.55	0.70	0.71	R0	0.82	0.82
2387[cu]	0.70	0.50	0.79	0.79	R0	0.80	0.70
2588[cu]	0.75	0.55	0.82	0.82	R0	0.90	0.90
2725[cu]	0.82	1.00	0.50	0.86	R1	0.90	0.90
U1							
2542[cu]	0.70	0.60	0.74	0.74	R0	0.80	0.80
2716[cu]	0.60	0.30	0.80	0.80	R0	0.80	0.60
2899[cu]	0.70	0.60	0.74	0.74	R0	0.90	0.90
I1							
3371[cu]	0.82	1.00	0.60	0.83	R1	0.90	0.90
3441[cu]	0.82	1.00	0.60	0.83	R1	0.95	0.95
3688[cu]	0.82	1.00	0.60	0.83	R1		
3908[cu]	0.85	1.00	0.65	0.86	R1	0.95	0.95
2/11-1							
3633[cu]	0.82	1.00	0.60	0.83	R1	0.90	0.90
3877[co]	0.85	1.00	0.55	0.88	R1	0.95	0.95
4548[cu]	0.85	1.00	0.65	0.86	R1	0.95	0.95
2/7-3							
3365[cu]	0.40	0.40	0.40	0.40	R0	0.75	0.75
3502[cu]	0.40	0.30	0.55	0.55	R0		
3789[cu]	0.95	1.00	1.00	1.00	R3	0.95	0.95
4178[cu]	0.90	1.00	0.70	0.91	R1	0.95	0.95
Lulu 1							
3420[cu]	0.85	1.00	0.55	0.88	R1	0.95	0.95
W1							
3816[cu]	0.50	0.40	0.60	0.60	R0	0.75	0.55
4051[cu]	0.80	1.00	0.45	0.85	R1		
Adda 1							
2633[cu]	0.65	0.45	0.76	0.76	R0		
2917[cu]	0.70	0.50	0.79	0.79	R0	0.85	0.85

[co] = core sample; [cu] = cuttings sample; P_I is the probability for an illite layer in illite/smectite (I/S); $P_{S.I}$ is the probability for an illite layer succeeding a smectite layer; $P_{SI.I}$ is the probability for an illite layer succeeding a SI sequence; $P_{SII.I}$ is the probability for an illite layer succeeding a SII sequence. Reichweite ordering after Reynolds (1984).

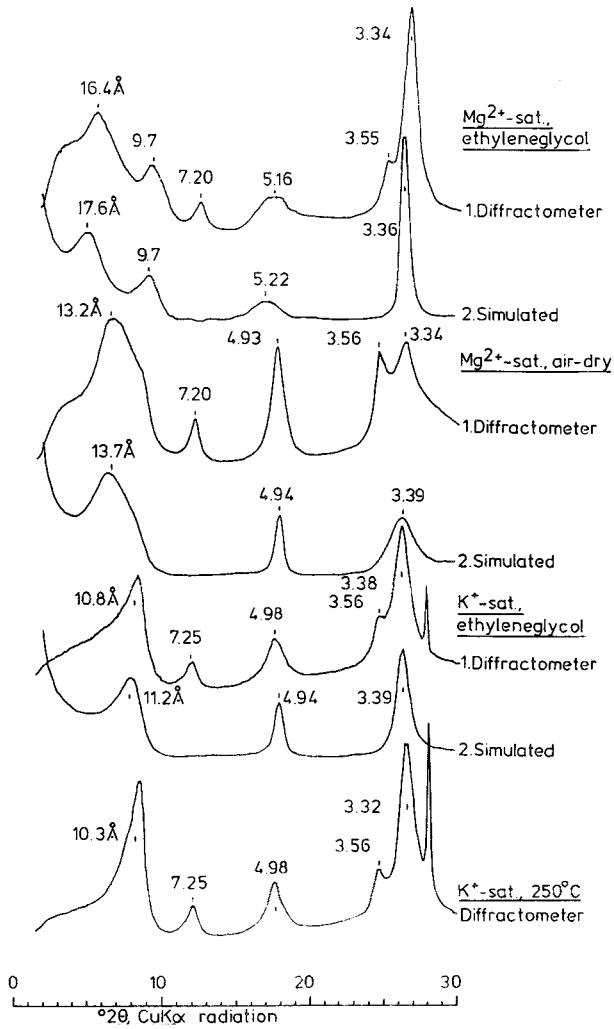


Figure 2. X-ray powder diffraction patterns and simulated patterns of oriented specimens of illite/smectite samples from well U1 (2542 m). The peaks at 7.2 and 3.5 Å are from kaolinite, the sharp peak at about 28°2θ is from KCl left from saturation. The Mg^{2+}-saturated and glycolated specimen was simulated with two glycol layers and: P_I (the probability for an illite layer in illite/smectite (I/S) = 0.7; $P_{S.I}$ (the probability for an illite layer succeeding a smectite layer) = 0.6; R (Reichweite) = 0 (for Reichweite ordering, see Reynolds, 1984). The Mg^{2+}-saturated and air-dry specimen was simulated with two water layers and P_I = 0.7, $P_{S.I}$ = 0.6, R = 0. The K^+-saturated and glycolated specimen was simulated with one glycol layer and P_I = 0.8, $P_{S.I}$ = 0.8, R = 0.

Table 1 and used throughout this paper. The I/S are R0-ordered for P_I = 0.40–0.75, R1-ordered for P_I = 0.80–0.90, and R3-ordered for P_I = 0.95. Initially the diffractograms were simulated with 0.3 Fe and 0.8 K mole per illite layer ($O_{10}(OH)_2$) and 0.4 CEC (cation-exchange capacity) and 0.3 Fe mole per smectite layer. Following the plots of chemical composition vs. P_I (Figure 7), the diffractograms were resimulated with 0.2 Fe and 0.6 K^+ (K^+ + 10/18 NH_4^+) per illite layer and 0.7 Fe and 0.7 CEC per smectite layer. Mg^{2+}-saturation and glycolation resulted in two interlayers for smectite and a d(001) of 17.0 Å, whereas K^+-saturation and glycolation resulted in one glycol layer between expandable layers and a d(001) of about 14.2 Å. These values were therefore used in the simulations. P_I values

https://doi.org/10.1346/CCMN.1991.0390108 Published online by Cambridge University Press

Table 2. X-ray powder diffraction data for 060 from illite/smectite samples from the North Sea.

Well	Depth (m)	P_I	Reichweite	d (060) (Å)	Halfwidth (Å)
E1	2983	0.65	R0	1.495	0.024
	3938	0.85	R1	1.499	0.020
M8	2368	0.65	R0	1.499	0.023
	2387	0.70	R0	1.496	0.024
U1	2542	0.70	R0	1.500	0.024
	2899	0.70	R0	1.499	0.023
I1	3908	0.85	R1	1.501	0.017
2/11-1	3877	0.85	R1	1.501	0.020
	4548	0.85	R1	1.501	0.020
2/7-3	3789	0.95	R3	1.499	0.016
Lulu 1	3420	0.85	R1	1.500	0.020
W1	3816	0.50	R0	1.499	0.023

P_I and Reichweite, see Table 1, footnote.

obtained from simulation of the K^+-saturated and glycolated specimens (Table 1) were markedly larger than those obtained from Mg^{2+}-saturated and air-dried or glycolated specimens. The relation between the P_I values for the glycolated K^+- and Mg^{2+}-saturated specimens is discussed below. Experimental and simulated diffractograms for the sample U1,2542m are shown in Figure 2.

The results of the XRD studies of randomly oriented samples are shown in Table 2. Quartz was used as a standard. XRD patterns of the 060 reflections of some I/S samples are shown in Figure 3. The position (center at half height) ranges between 1.499 and 1.501 Å, and the half width ranges from 0.016 to 0.024 Å. No splitting of the 060 reflection was observed.

Separate 060 reflection from kaolinite was also not observed; however, the invariance of the kaolinite content with P_I suggests that the changes in d(060) with P_I are attributable to changes in d(060) of illite and smectite layers in I/S.

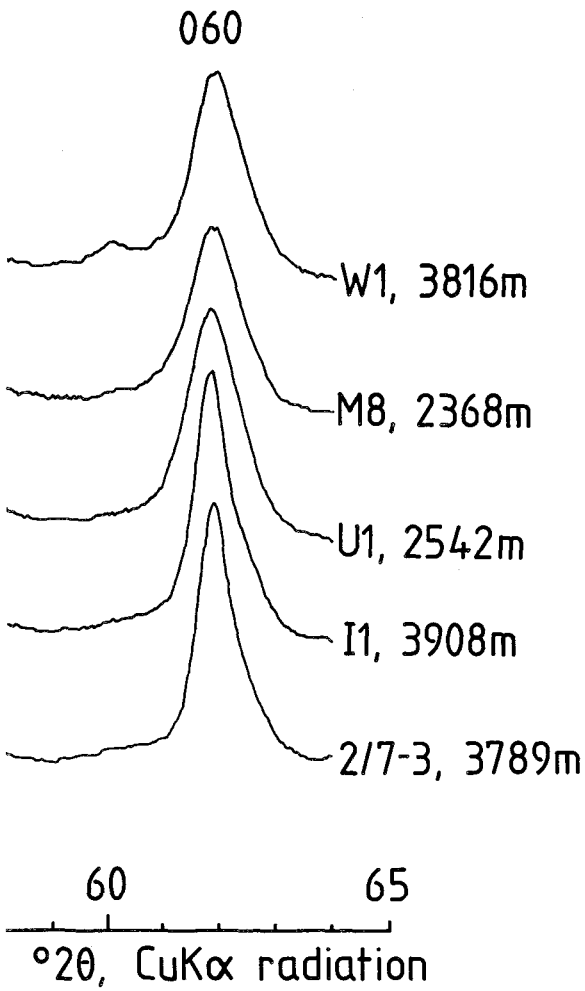


Figure 3. X-ray powder diffraction patterns of the 060 reflection of randomly oriented specimens of some illite/smectite samples. The peak at about 60°2θ is probably a kaolinite peak ($2\bar{2}4$,$1\bar{3}4$,$31\bar{3}$,203).

^{27}Al and ^{29}Si MAS-NMR spectroscopy

The ^{27}Al and ^{29}Si chemical shifts determined for the North Sea clay samples are summarized in Table 3. As a typical example of the high-quality ^{27}Al NMR spectra obtained for the clay samples in this study, Figure 4 shows the ^{27}Al MAS spectrum for sample 2/7-3,3789m recorded at a spinning speed of 13.5 kHz. The spectrum illustrates that the high and stable spinning speeds, achievable with the homebuilt MAS probes, allowed spinning sidebands to be moved completely outside the regions for the Al^{IV} (71.2–73.6 ppm) and Al^{VI} (4.9–6.1 ppm) resonances at both 7.1 and 9.4 T magnetic field strengths. Obviously, such spectra greatly facilitate quantitative determination of Al^{IV}/Al^{VI} ratios from spectral deconvolution (Table 4), compared with earlier published low-speed spinning ^{27}Al MAS spectra (Thompson, 1984). Furthermore, the spectrum shows that, in addition to the ^{27}Al *central* ($m = +1/2 \leftrightarrow m = -1/2$) transitions, spinning sideband manifolds for the *inner* satellite ($m = \pm 3/2 \leftrightarrow m = \pm 1/2$) transitions were also observed. Using the theoretical procedure outlined by Samoson (1985), these sidebands allowed the SOQE = $(QCC)(1 + \eta^2/3)^{1/2}$ parameters (where QCC = quadrupole coupling constant, and η = asymmetry parameter) and, thus, "corrected" ^{27}Al chemical shifts to be determined (Table 3). For the samples of the present study, the SOQE values were in the ranges 2.3–3.0 MHz and 1.8–2.6 MHz for the Al^{IV} and Al^{VI} sites, respectively; they were thus of similar magnitude for the two sites. Along with the experimental conditions employed (e.g., Al background-free probe, small flip angle, sufficient relaxation delay, high spinning speeds), the similar magnitudes of the quadrupole coupling parameters for the Al^{IV} and Al^{VI} sites ensured that Al^{IV}/Al^{VI} ratios were determined with high accuracy.

https://doi.org/10.1346/CCMN.1991.0390108 Published online by Cambridge University Press

Table 3. ^{27}Al and ^{29}Si chemical shifts[1] of illite/smectite samples from the North Sea.

Well	Depth (m)	$\delta(^{29}Si(0Al))$	$\delta(^{29}Si(1Al))$	$\delta(^{29}Si(2Al))$	$\delta(^{27}Al^{IV})$	$\delta(^{27}Al^{VI})$
G1	2609	−93.7	−88.3	−85.0	73.6	6.1
M8	2368	−93.3	−86.2	−83.6	71.3	5.0
U1	2899	−93.4	−87.1	−82.9	71.4	5.1
2/7-3	3365	−93.3	−86.2	−84.5	71.3	5.0
G1	3441	−94.1	−87.6	−85.4	73.3	6.1
U1	2542	−92.9	−86.3	−83.8	72.1	5.5
M8	2588	−93.0	−87.7	−83.4	72.2	5.7
2/7-3	3502	−92.9	−87.5	−83.4	73.1	5.8
M8	2725	−93.0	−87.6	−83.9	72.8	5.4
E1	3938	−93.7	−87.0	−83.8	71.2	5.0
Lulu 1	3420	−93.2	−86.9	−83.1	71.6	4.9
2/11-1	4548	−93.0	−87.0	−84.0	71.5	5.2
2/11-1	3877	−93.0	−87.7 to −86.0	−82.3	72.7	5.9
2/7-3	3789	−93.4	−87.2	−82.0	72.8	6.0

[1] ^{27}Al chemical shifts are in ppm (±0.5 ppm) referenced to external $Al(H_2O)_6^{3+}$, for a 1 M solution of $AlCl_3$ in H_2O. ^{29}Si chemical shifts are in ppm (±0.5 ppm) referenced to external TMS.

For the ^{29}Si MAS-NMR spectra of the North Sea I/S clays, the centerband resonance of this spin I = 1/2 nucleus was resolved into separate ^{29}Si resonances corresponding to the number of nearest Al^{IV} in the I/S layers, i.e., $Si[Al(4)]_n[Si]_{3-n}$, where n = 0, 1, and 2 (Jakobsen *et al.*, 1988b). The ranges observed for the samples in the present study (Table 3) ($\delta^{29}Si(0Al) \approx -92$ to -95 ppm; $\delta^{29}Si(1Al) \approx -86$ to -89 ppm; and $\delta^{29}Si(2Al) \approx -82$ to -86 ppm) were used to deconvolute the ^{29}Si MAS spectra. Illustrative examples of ^{29}Si MAS spectra, representing I/S clays having different Si/Al^{IV} ratios, are shown in Figure 5. The intensities of the Si(nAl) resonances, $I_{Si(nAl)}$, determined from the spectral deconvolutions were used to calculate the Si/Al^{IV} ratios (Table 4) according to Eq. (1). The general trend of the data in Table 4 is that the Si/Al^{IV} ratio decreased with increasing Al^{IV}/Al^{VI} ratio, as would be expected.

Mössbauer spectroscopy

The Mössbauer spectra were computerfitted with five quadrupoles, three Fe^{3+} doublets and two Fe^{2+} doublets, as this number gave satisfactory fits. The results show that the area ratios of the Fe-components were independent of temperature; thus, the f-factors were identical. Johnston and Cardile (1985), however, found that different interlayer cations changed the recoilless fractions (f-factors) in nontronites. Therefore, K^+-fixation during illite layer formation should change the recoilless fractions in I/S. This change was not observed in the present investigation. Because the f-factors were identical for the different spectral components, their relative areas were taken as relative percentages of the Fe-components. Differences between spectra obtained with the absorber plane normal to and at an angle of 54.7° to the radiation were not significant; hence, texture effects were negligible.

Mössbauer parameters for the I/S at room temperature are summarized in Table 5; the spectra are shown in Figure 6. Visually the spectra are almost identical for the five I/S samples. A broad (Γ = 0.6 mm/s) Fe^{3+}

Table 4. Si/Al^{IV} and Al^{IV}/Al^{VI} ratios determined from deconvolution of ^{29}Si and ^{27}Al nuclear magnetic resonance spectra of illite/smectite samples from the North Sea.

Well	Depth (m)	Si/Al^{IV}	Al^{IV}/Al^{VI}
G1	2609	11.7	0.17
M8	2368	11.2	0.21
U1	2899	11.0	0.21
2/7-3	3365	10.7	0.23
G1	3441	10.1	0.22
U1	2542	9.6	0.24
M8	2588	8.9	0.19
2/7-3	3502	8.3	0.23
M8	2725	7.8	0.21
E1	3938	7.5	0.27
Lulu 1	3420	7.3	0.27
2/11-1	4548	6.4	0.34
2/11-1	3877	5.8	0.35
2/7-3	3789	5.0	0.38

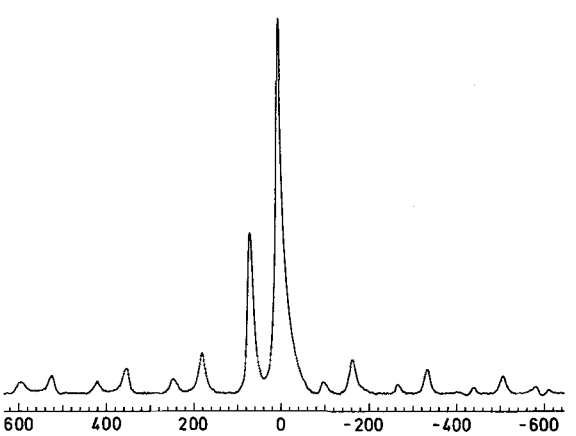


Figure 4. High-speed ^{27}Al magic-angle spinning (MAS)-nuclear magnetic resonance (NMR) spectrum of illite/smectite sample from well 2/7-3 (3789 m) from the North Sea. Spectrum was recorded at 78.16 MHz and with rotor (Si_3N_4) speed of 13.5 kHz.

https://doi.org/10.1346/CCMN.1991.0390108 Published online by Cambridge University Press

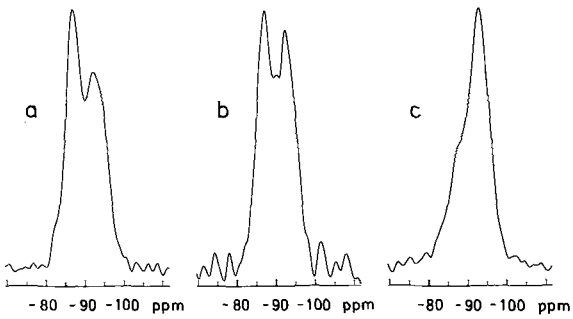


Figure 5. High-speed ^{29}Si magic-angle spinning (MAS)-nuclear magnetic resonance (NMR) spectra of illite/smectite samples from the North Sea. Spectra were recorded at 59.59 MHz with rotor (PSZ) speeds of ~7.2 kHz. (a) Spectrum for sample from well 2/7-3 (3789 m) (Si/Al = 5.0). (b) Spectrum for sample from well 2/11-1 (3877 m) (Si/Al = 5.8). (c) Spectrum for sample from well U1 (2899 m) (Si/Al = 11.0).

doublet and a narrower (Γ = 0.3 mm/s) Fe^{2+} doublet account for about 80% and 15% of the absorption area, respectively, for all spectra. Therefore, the spectral parameters (Table 5) for these two doublets are statistically reliable. Assignment of the components of the Mössbauer spectra to Fe^{2+} or Fe^{3+} in various crystallographic sites has been extensively discussed in the literature. Lately, Goodman (1987) and Cardile (1987) argued that each crystallographic site will produce several doublets having different Mössbauer parameters because of long-range contributions to the electric field gradients. In clay minerals low in iron, such as those investigated here, a considerable variation existed in the nearest and more distant surrounding cations, which should have produced broad peaks, as observed for the major Fe^{3+} component. The d(060) value of 1.499–1.501 Å shows that the I/S were dioctahedral. Thus, the main Fe^{3+} doublet (isomer shift δ = 0.32–0.34 mm/s, quadrupole splitting Δ = 0.49–0.56 mm/s) and the main Fe^{2+} doublet (δ = 1.13–1.15 mm/s, Δ = 2.80–2.88 mm/s) must be assigned to octahedral Fe, inasmuch as the values correspond to those given for octahedral Fe^{2+} and Fe^{3+} by Goodman (1976) for muscovite. The spectral parameters of the three remaining components (<5%) fitted to the spectra are very uncertain (Table 5). Within experimental uncertainties, the values for δ, Δ, Γ, and amount (%) for the main Fe^{3+} component are identical for all samples. Similarly, the δ and Δ values for the main Fe^{2+} component are identical for all samples, whereas Γ and the percentage of this Fe^{2+} component are lower in samples 2/11-1,3877m and M8,2368m, compared with samples U1,2899m, 2/7-3,3365m, and 2/7-3,3789m. These differences are, however, not related to different P_f values or to ordering values for these samples.

Total chemical analysis

Total chemical analysis of Na^+-saturated I/S samples are shown in Table 6. The presence of NH_4^+ was also seen by IR, from the bands at 1410–1430 and at 3300

Table 5. Mössbauer data for illite/smectite samples from the North Sea.

Well (Depth (m))		δ (mm/s)	Δ (mm/s)	Γ (mm/s)	Area (%)
U1	Fe^{3+}	0.34 ± 0.003	0.56 ± 0.003	0.57 ± 0.009	78.3 ± 0.06
(2899)	Fe^{3+}	0.40 ± 0.03	1.24 ± 0.03	0.26 ± 0.07	3.4 ± 0.05
	Fe^{3+}	0.08 ± 0.15	0.53 ± 0.15	0.32 ± 0.43	0.8 ± 0.05
	Fe^{2+}	1.13 ± 0.01	2.80 ± 0.01	0.38 ± 0.03	14.2 ± 0.05
	Fe^{2+}	1.37 ± 0.09	1.69 ± 0.09	0.67 ± 0.26	3.3 ± 0.06
M8	Fe^{3+}	0.32 ± 0.01	0.56 ± 0.01	0.57 ± 0.02	79.8 ± 0.03
(2368)	Fe^{3+}	0.62 ± 0.23	1.84 ± 0.23	0.97 ± 0.65	3.9 ± 0.04
	Fe^{3+}	0.06 ± 0.04	0.51 ± 0.04	0.15 ± 0.10	2.1 ± 0.02
	Fe^{2+}	1.15 ± 0.02	2.86 ± 0.02	0.27 ± 0.05	9.0 ± 0.03
	Fe^{2+}	1.67 ± 0.04	1.36 ± 0.04	0.29 ± 0.10	4.8 ± 0.03
2/11-1	Fe^{3+}	0.34 ± 0.01	0.49 ± 0.01	0.57 ± 0.02	81.2 ± 0.05
(3877)	Fe^{3+}	0.43 ± 0.06	1.24 ± 0.06	0.13 ± 0.17	2.1 ± 0.04
	Fe^{3+}	0.05 ± 0.12	0.47 ± 0.12	0.09 ± 0.35	0.7 ± 0.04
	Fe^{2+}	1.13 ± 0.02	2.88 ± 0.02	0.27 ± 0.07	11.7 ± 0.05
	Fe^{2+}	1.29 ± 0.15	1.51 ± 0.15	0.58 ± 0.42	4.3 ± 0.05
2/7-3	Fe^{3+}	0.34 ± 0.01	0.53 ± 0.01	0.64 ± 0.03	79.4 ± 0.04
(3365)	Fe^{3+}	0.81 ± 0.47	2.25 ± 0.47	0.54 ± 1.33	1.5 ± 0.04
	Fe^{3+}	0.10 ± 0.05	0.73 ± 0.05	0.05 ± 0.15	1.1 ± 0.03
	Fe^{2+}	1.13 ± 0.03	2.81 ± 0.03	0.37 ± 0.09	15.4 ± 0.04
	Fe^{2+}	1.74 ± 0.09	1.23 ± 0.09	0.19 ± 0.24	2.6 ± 0.04
2/7-3	Fe^{3+}	0.33 ± 0.01	0.56 ± 0.01	0.63 ± 0.03	76.3 ± 0.07
(3789)	Fe^{3+}	0.60 ± 0.24	1.76 ± 0.24	0.25 ± 0.69	1.3 ± 0.07
	Fe^{3+}	0.00 ± 0.07	0.30 ± 0.07	0.10 ± 0.20	1.8 ± 0.07
	Fe^{2+}	1.15 ± 0.02	2.86 ± 0.02	0.30 ± 0.06	16.9 ± 0.07
	Fe^{2+}	1.62 ± 0.12	1.22 ± 0.12	0.36 ± 0.34	3.7 ± 0.07

δ = isomer shift; Δ = quadrupole splitting; Γ = halfwidth.

https://doi.org/10.1346/CCMN.1991.0390108 Published online by Cambridge University Press

Table 6. Total chemical analysis (% oxides) by atomic absorption spectrophotometry of illite/smectite samples from the North Sea.

Well	Depth (m)	$(NH_4)_2O$	Na_2O	K_2O	CaO	MgO	Fe_2O_3	Al_2O_3	SiO_2	P_I	$P_{S.I}$	R
E1	3938		3.73	4.66	0.31	2.38	5.94	27.4	55.6	0.85	0.99	R1
G1	2609		4.70	3.97	0.48	2.81	6.94	24.6	56.5	0.75	0.65	R0
M8	2368	0.23	4.56	4.21	0.29	3.07	6.06	24.9	56.9	0.65	0.55	R0
U1	2542	0.32	4.13	4.28	0.22	2.92	7.36	24.9	56.3	0.70	0.60	R0
	2716	0.32	5.18	3.46	0.14	3.51	7.07	23.9	56.8	0.60	0.30	R0
	2899	0.52	4.38	4.39	0.15	3.12	5.71	25.7	56.5	0.70	0.60	R0
I1	3371		3.97	4.01	0.19	2.02	4.69	29.7	55.4	0.82	0.99	R1
	3908	1.20	4.08	4.90	0.16	2.69	4.17	27.9	56.1	0.85	0.99	R1
2/11-1	3877	1.38	4.13	4.58	0.03	1.72	4.23	30.1	55.2	0.85	0.99	R1
	4548		4.46	4.62	0.32	2.07	6.02	28.0	54.5	0.85	0.99	R1
2/7-3	3365	0.27	4.94	2.96	0.12	2.48	5.89	25.6	58.1	0.40	0.40	R0
	3789	1.54	3.93	5.04	0.49	1.49	3.34	32.1	53.6	0.95	0.99	R3
	4178	0.62	3.82	5.15	0.19	1.78	3.80	30.2	55.1	0.90	0.99	R1
Lulu 1	3420		4.12	5.35	0.10	2.34	5.26	28.8	54.0	0.85	0.99	R1
Adda 1	2917		4.43	3.59	0.27	2.61	8.05	25.6	55.4	0.70	0.50	R0
W1	3816	0.41								0.50	0.40	R0

R is Reichweite. For P_I, $P_{S.I}$, and Reichweite, see Table 1, footnotes.

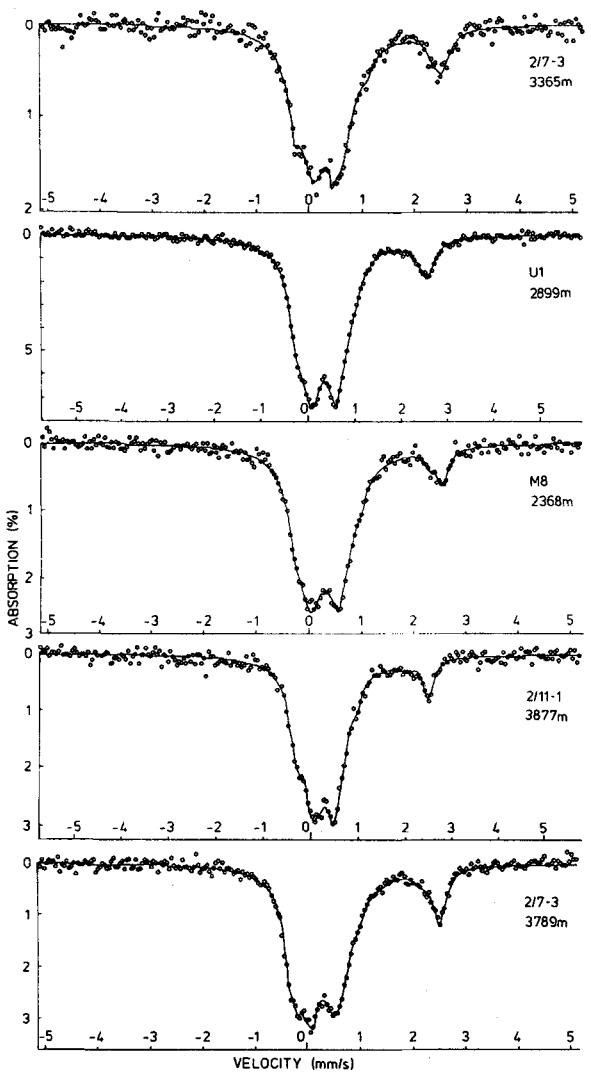


Figure 6. Mössbauer spectra of illite/smectite samples analyzed at room temperature. Experimental spectra = open circles; simulated spectra = solid lines.

cm^{-1} and the increase in the intensity of these bands with increasing amounts of NH_4^+, as determined by isotopic dilution. NH_4-containing illites were described by Higashi (1978) and Sterne *et al.* (1982). Small but significant amounts of Ca were detected in all samples. This Ca must be fixed between layers, because no Ca minerals were detected by either XRD or differential thermal analysis with detection of evolved CO_2 and because the exchangeable cations have been exchanged by Na^+.

Analysis of NH_4^+-saturated fine-clay fractions showed only traces of Na^+. Therefore, the Na^+ determined in Na^+-saturated samples (Table 6) must chiefly be adsorbed on exchangeable sites (between expandable layers and at particle edges).

The mixed-layer formulae in Table 7 were calculated based on the following assumptions: (1) the ideal cell contained two octahedral and four tetrahedral cations per $O_{10}(OH)_2$ unit; and (2) Na^+, K^+, NH_4^+, and Ca^{2+} were present as interlayer cations, Mg^{2+}, Fe^{2+}, and Fe^{3+} as octahedral cations, Si^{4+} as tetrahedral cations, and Al^{3+} as both octahedral and tetrahedral cations. The Al^{IV}-occupancy was calculated as (4 − Si), and therefore the relative error in Al^{IV} is given by Si/Al^{VI} (relative error in Si). Assuming an analytical error in Si of 5%, the relative error in Al^{IV} was about 35%. Therefore, the I/S formulae calculated from the AAS data were considered inaccurate. According to the formulae in Table 7, the dominating octahedral cation was Al^{VI}, and part of the negative layer charge arose from tetrahedral Al^{IV}-for-Si substitution. Generally, a surplus

https://doi.org/10.1346/CCMN.1991.0390108 Published online by Cambridge University Press

Table 7. Illite/smectite formulae calculated from atomic absorption spectrophotometry (AAS) data (Table 6) for illite/smectite samples from the North Sea.[1]

Well	Depth (m)	Framework
E1	3938	$Na_{0.45}K_{0.37}Ca_{0.02}(Mg_{0.22}Fe_{0.28}Al_{1.50})(Al_{0.52}Si_{3.48})$
G1	2609	$Na_{0.58}K_{0.32}Ca_{0.03}(Mg_{0.27}Fe_{0.33}Al_{1.39})(Al_{0.44}Si_{3.56})$
M8	2368	$(NH_4)_{0.03}Na_{0.56}K_{0.34}Ca_{0.02}(Mg_{0.29}Fe_{0.29}Al_{1.42})(Al_{0.42}Si_{3.58})$
U1	2542	$(NH_4)_{0.05}Na_{0.50}K_{0.34}Ca_{0.02}(Mg_{0.27}Fe_{0.35}Al_{1.38})(Al_{0.46}Si_{3.54})$
	2716	$(NH_4)_{0.05}Na_{0.63}K_{0.28}Ca_{0.01}(Mg_{0.33}Fe_{0.34}Al_{1.33})(Al_{0.44}Si_{3.56})$
	2899	$(NH_4)_{0.08}Na_{0.53}K_{0.35}Ca_{0.01}(Mg_{0.29}Fe_{0.27}Al_{1.44})(Al_{0.46}Si_{3.54})$
I1	3371	$Na_{0.48}K_{0.32}Ca_{0.01}(Mg_{0.19}Fe_{0.22}Al_{1.60})(Al_{0.57}Si_{3.43})$
	3908	$(NH_4)_{0.17}Na_{0.50}K_{0.39}Ca_{0.01}(Mg_{0.25}Fe_{0.20}Al_{1.55})(Al_{0.50}Si_{3.50})$
2/11-1	3877	$(NH_4)_{0.20}Na_{0.50}K_{0.36}Ca_{0.00}(Mg_{0.16}Fe_{0.20}Al_{1.64})(Al_{0.56}Si_{3.44})$
	4548	$Na_{0.55}K_{0.37}Ca_{0.02}(Mg_{0.19}Fe_{0.28}Al_{1.52})(Al_{0.56}Si_{3.44})$
2/7-3	3365	$(NH_4)_{0.02}Na_{0.59}K_{0.24}Ca_{0.01}(Mg_{0.23}Fe_{0.28}Al_{1.48})(Al_{0.39}Si_{3.61})$
	3789	$(NH_4)_{0.22}Na_{0.48}K_{0.40}Ca_{0.03}(Mg_{0.14}Fe_{0.16}Al_{1.70})(Al_{0.66}Si_{3.34})$
	4178	$(NH_4)_{0.09}Na_{0.46}K_{0.41}Ca_{0.01}(Mg_{0.16}Fe_{0.18}Al_{1.66})(Al_{0.56}Si_{3.44})$
Lulu 1	3420	$Na_{0.50}K_{0.34}Ca_{0.01}(Mg_{0.22}Fe_{0.25}Al_{1.53})(Al_{0.60}Si_{3.40})$
Adda 1	2917	$Na_{0.54}K_{0.29}Ca_{0.02}(Mg_{0.25}Fe_{0.38}Al_{1.37})(Al_{0.52}Si_{3.48})$

[1] The uncertainty in the determination of Al(IV) contents from the AAS data (see text) along with the presence of ~5% kaolinite limits the mineralogical significance of the total formulae. They are, however, useful for comparison with the nuclear magnetic resonance results.

of interlayer cations compared with the total negative layer charge resulting from octahedral and tetrahedral substitutions is suggested by the formulae in Table 7. This surplus may have been due to cation adsorption at particle edges. Finally, it should be noted that the I/S samples contained a small amount (~5%) of kaolinite.

DISCUSSION

Comparison of data from chemical analysis and NMR

The Si/Al^{IV} and Al^{IV}/Al^{VI} ratios determined from deconvolution of the ^{29}Si and ^{27}Al MAS spectra and calculated from the AAS analyses are summarized in Table 8. Also included in Table 8 are the results for the Si/Al (Al = Al^{IV} + Al^{VI}) ratios calculated from the NMR data and AAS analysis. Because of the error in Al^{IV} calculated from AAS (see above) the errors in the Si/Al^{IV} and Al^{IV}/Al^{VI} ratios are high (2–3 and about 0.1, respectively). Fair agreement, however, was noted between the ratios calculated from the AAS data and those determined from the NMR spectra. The Si/Al ratios determined from AAS were considerably more accurate (about 10% accuracy) than those calculated from AAS for Si/Al^{IV} and Al^{IV}/Al^{VI}. The correlation between the Si/Al ratios from AAS and NMR was high ($r = 0.97$), and, thus, this ratio was probably determined with high accuracy by both methods. The agreement between the AAS and NMR Si/Al ratios shows that the Si/Al^{IV} and Al^{IV}/Al^{VI} ratios were determined from NMR with satisfactory accuracy. On the other

Table 8. Comparison of Si/Al ratios in illite/smectite samples from the North Sea determined from atomic absorption spectrophotometry (AAS) and nuclear magnetic resonance spectroscopy (NMR).

		Si/Al^{IV}		Al^{IV}/Al^{VI}		Si/Al[3]	
Well	Depth (m)	AAS[1]	NMR[2]	AAS	NMR	AAS	NMR
E1	3938	7	7.5	0.3	0.27	1.7	1.60
G1	2609	8	11.7	0.3	0.17	1.9	1.72
	3441		10.1		0.22		1.78
M8	2368	9	11.2	0.3	0.21	1.9	1.90
	2588		8.9		0.19		1.43
	2725		7.8		0.21		1.37
U1	2542	8	9.6	0.3	0.24	1.9	1.87
	2899	8	11.0	0.3	0.21	1.9	1.90
2/11-1	3877	6	5.8	0.3	0.35	1.6	1.50
	4548	6	6.4	0.4	0.34	1.7	1.64
2/7-3	3365	9	10.7	0.3	0.23	1.9	2.02
	3502		8.3		0.23		1.52
	3789	5	5.0	0.4	0.38	1.4	1.38
Lulu 1	3420	6	7.3	0.4	0.27	1.6	1.55

[1] Ratio determined by total chemical analysis by AAS.
[2] Ratio determined by NMR spectroscopy.
[3] The Si/Al ratio represents the ratio $Si/(Al^{IV} + Al^{VI})$.

https://doi.org/10.1346/CCMN.1991.0390108 Published online by Cambridge University Press

hand, the low accuracy of the Si/Al^{IV} and Al^{IV}/Al^{VI} ratios calculated from the AAS data is evident from Table 8.

Finally, mutual agreement between the Al^{IV}/Al^{VI} and Si/Al^{IV} ratios determined from ^{27}Al and ^{29}Si MAS NMR, respectively, was also suggested by the increase in the Al^{IV}/Al^{VI} ratio, i.e., greater substitution of Al^{3+}-for-Si^{4+} in the tetrahedral sheet, was accompanied by a decrease in the Si/Al^{IV} ratio (Table 4).

Lattice transformation during illite layer formation

Interlayer cations. Considerable K and NH_4 were found in samples having a high Al-content (Table 6), probably because K^+ and NH_4^+ are fixed between the 2:1 layers if the negative charge resulting from tetrahedral $^{IV}Al^{3+}$-for-Si^{4+} substitution is sufficiently high. Plots of % $(NH_4)_2O$, % K_2O, and % Na_2O vs. P_I are shown in Figures 7A–7C. Adsorbed Na^+ decreased and fixed K^+ and, particularly, NH_4^+ increased with increasing P_I. Altogether, an increase in interlayer cations (moles of $Na^+ + K^+ + NH_4^+$) with increasing P_I was observed (Figure 7H). Fixation of K^+ and NH_4^+ during illite layer formation thus resulted in a decrease in CEC. Fixed ($K^+ + NH_4^+$) is plotted against P_I in Figure 7H; the curves of Hower and Mowatt (1966) and Środoń *et al.* (1986) for fixed K^+ vs. amount of illite layers are shown for comparison. These two line segments are roughly parallel to the line segment drawn in the present investigation. They suggest, however, that the I/S of Hower and Mowatt (1966) and Środoń *et al.* (1986) contain per $O_{10}(OH)_2$ about 0.05 K^+ more than $K^+ + NH_4^+$ amounts to in the present investigation at the same P_I values. The range of P_I values covered by the investigation of Środoń *et al.* (1986) permits conclusions to be drawn for the range 0–1.0 P_I. Środoń *et al.* (1986) proposed a kinked line with kinking at P_I = 0.55. The data of the present investigation were only statistically reliable at P_I values >0.5 and therefore could not give similar information.

I/S containing 80% illite layers from the Pleistocene to Eocene Gulf Coast sediments contain 4–5% K_2O (Perry and Hower, 1972). Similarly, I/S containing 80% illite layers from Oligocene to Miocene Gulf Coast sediments contain about 5.5% K_2O (Hower *et al.*, 1976). Late Cretaceous to Late Triassic I/S containing 20% smectite layers from the Canadian Sverdrup Basin contain 6.43% K_2O (Foscolos and Powell, 1979). These percentages are greater than the 4.5% K_2O at P_I = 0.8 found in the present investigation, but agree with the total amount of fixed cations found by us at this P_I value [4.5% K_2O + $(NH_4)_2O$ equivalent to 1.5% K_2O].

Extrapolation of the plots in Figure 7 to P_I = 1.0 (100% illite layers) resulted in 5.3% K_2O and in an $(NH_4)_2O$ amount equivalent to 2.8% K_2O for I/S. This agrees well with the illite samples investigated by Hower and Mowatt (1966), but it is still far from that of micas (10%; Deer *et al.*, 1967). Thus, about 20% of the illite interlayer sites probably contained no fixed K^+ or NH_4^+.

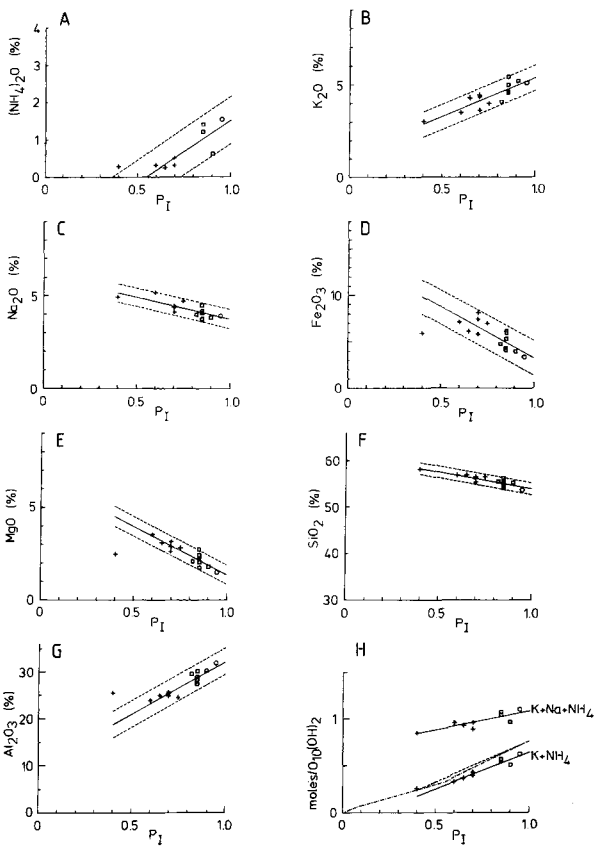


Figure 7. Elemental composition of illite/smectite samples plotted against P_I. Symbols in A–G: Solid lines are regression lines, dotted lines delimit two standard deviations, + = R0-ordered, □ = R1-ordered, and ○ = R3-ordered. A = $\%(NH_4)_2O$ vs. P_I; correlation coefficient of 0.83. B = $\%K_2O$ vs. P_I; correlation coefficient of 0.87. C = $\%Na_2O$ vs. P_I; correlation coefficient of 0.81. D = $\%Fe_2O_3$ vs. P_I; point at 0.4 omitted in the regression analysis; correlation coefficient of −0.79. E = %MgO vs. P_I; point at 0.4 omitted in the regression analysis; correlation coefficient of −0.90. F = $\%SiO_2$ vs. P_I; correlation coefficient of −0.87. G = $\%Al_2O_3$ vs. P_I; point at 0.4 omitted in the regression analysis; correlation coefficient of 0.86. H = equivalents of NH_4^+, K^+, and Na^+ per $O_{10}(OH)_2$ vs. P_I; symbols for ordering as in A–G; solid lines are regression lines (omitting the point at P_I 0.4 for $K^+ + NH_4^+$). ·-·-· = line of Środoń *et al.* (1986); ----- = line of Hower and Mowatt (1968); correlation coefficient for $(NH_4 + K + Na)$ vs. P_I is 0.82; correlation coefficient for $(NH_4 + K)$ vs. P_I is 0.95.

Tetrahedral and octahedral cations. The variations in the percentages of Fe_2O_3, MgO, SiO_2, and Al_2O_3 with P_I are shown in Figures 7D–7G, respectively. Fe_2O_3, MgO, and SiO_2 decrease, whereas Al_2O_3 increases with increasing P_I. These Si, Mg, and Al trends are similar to those found by Hower *et al.* (1976) for the Gulf Coast Oligocene-Miocene sediments. I/S from sample 2/7-3,3365m deviated significantly from the general

https://doi.org/10.1346/CCMN.1991.0390108 Published online by Cambridge University Press

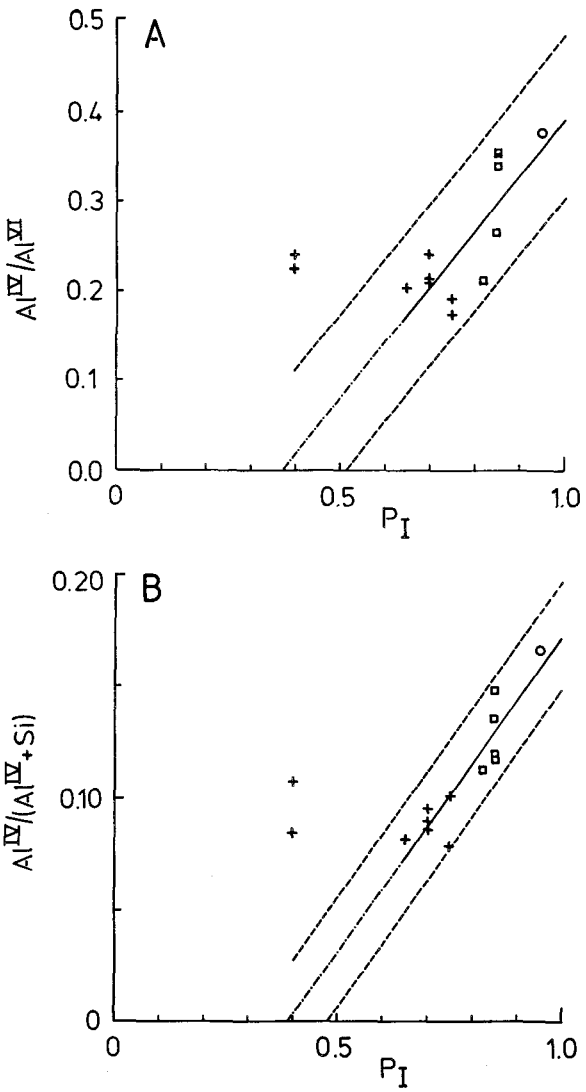


Figure 8. A = illite/smectite (I/S) sample Al^{IV}/Al^{VI} ratios (from ^{27}Al nuclear magnetic resonance (NMR) spectroscopy) vs. P_I; correlation coefficient of 0.80. B = $Al^{IV}/(Al^{IV} + Si)$ I/S ratios (from ^{29}Si NMR) vs. P_I; correlation coefficient of 0.91. Solid lines are regression lines; dotted lines delimit two standard deviations. The two points at P_I 0.4 have been omitted from the regression analysis.

trend in containing less Mg and Fe and more Al. From NMR, this sample had a higher tetrahedral charge compared with the other I/S samples. These deviations may be due to different parent material for the I/S. Hansen and Lindgreen (1989) concluded that this sample is a bentonite originating from volcanic ash, whereas the other samples originate from detrital, R0-ordered I/S with P_I ~0.65. According to Velde and Brusewitz (1986), I/S originating from volcanic ash has a larger tetrahedral charge than I/S in shales. Thus, the chemical results of the present investigation suggest that the I/S in sample 2/7-3,3365m formed from volcanic ash.

Finally, as mentioned above, the kaolinite content did not vary with P_I and thus did not influence the observed increase in Al^{VI} with increasing P_I.

Mössbauer spectroscopy showed Fe to be chiefly in octahedral positions. The Fe^{2+}/Fe^{3+} ratio did not vary significantly with P_I or degree of ordering, even if the I/S in which $P_I = 0.95$ and ordering = R3 from sample 2/7-3,3789m contained more Fe^{2+} (21%) compared with the other I/S samples (14–18%). Generally, the apparent lack of variation in the Mössbauer spectral parameters for the octahedral Fe^{2+} and Fe^{3+} with P_I indicate that the octahedral sheet did not change during formation of the illite layers. Mössbauer chemical shifts and quadrupole splitting for the I/S from sample 2/7-3,3365m, however, did not deviate significantly from those of the four other samples investigated by Mössbauer spectroscopy, despite the fact that this sample was of presumeably different (volcanic) origin. Therefore, the broadness of the dominating Fe^{3+} component may have made detection of an octahedral variation difficult. The loss of octahedral Fe and Mg may have been balanced by Al, which is in full agreement with the Al and Si tetrahedral and octahedral occupancies determined from NMR (Table 4). The AAS formulae (Table 7) and the increase in the Al^{IV}/Al^{VI} and $Al^{IV}/(Al^{IV} + Si)$ ratios with increasing P_I (Figures 8A and 8B show that the increase in Al took place by Al-substitution in both the octahedral and tetrahedral sheets.

Powers (1959) and Dunoyer de Segonzac (1970) proposed that an increase in P_I is accompanied by a migration of Al from octahedral to tetrahedral sites; hydrothermal experiments by Frank-Kamenetski *et al.* (1979) supported this proposal. Contrarily, Howard (1981) found that Al^{VI} remained constant in I/S from shales and sandstones as Al^{IV} increased, and Środoń *et al.* (1986) calculated that the octahedral charge remained constant during illite layer formation. The increase in Al^{VI} and decrease in octahedral Mg and Fe observed with increasing P_I for the present I/S does not conform with the results of Frank-Kamenetski *et al.* (1979), Howard (1981), or Środoń *et al.* (1986). This could be due to the fact that a calculation of octahedral Al from NMR (used in our investigation) is more accurate (see above) than a calculation from the total Al and Si content (used by these authors). It could also be due to differences in parent material and solution chemistry of the rocks.

Dimensional lattice changes during illite layer formation. The *b*-dimension of the 2:1 unit as estimated from the position of the 060 reflection did not change with P_I, % Al_2O_3, or the Si/Al^{IV} ratio determined by NMR; however, the halfwidth decreased linearly with P_I and % Al_2O_3 and increased linearly with the Si/Al^{IV} ratio.

A continuous octahedral sheet constrains the geometry of an attached tetrahedral sheet (Guggenheim

https://doi.org/10.1346/CCMN.1991.0390108 Published online by Cambridge University Press

and Eggleton, 1987). The unconstrained tetrahedral sheet dimensions are probably larger than the corresponding octahedral dimensions (Bailey, 1984). The fit between a "larger" tetrahedral sheet and a "smaller" octahedral sheet can be brought about by rotation of tetrahedra (Radoslovich, 1961). The lateral dimension of the octahedral sheet can be calculated from: $b_{oct} = 3(M\text{–}O)\sqrt{2}$, where M–O represents the mean octahedral cation-oxygen distance, and an unconstrained lateral dimension of the tetrahedral sheet from: $b(Si_{1-x}Al_x) \approx 9.15 + 0.74x$ (Guggenheim and Eggleton, 1987). The degree of tetrahedral rotation α may be calculated from: $\cos\alpha = b_{meas}/b_{ideal}$ (Weiss *et al.*, 1987), where b_{meas} is estimated from d(060) and b_{ideal} is calculated from $b(Si_{1-x}Al_x) \approx 9.15 + 0.74x$. The following values can be calculated for I/S with $P_I = 0.5$ and $P_I = 0.95$ in the present investigation:

$$\begin{aligned} P_I = 0.50&: b_{oct} = 8.35\ \text{Å}\ b(Si_{1-x}Al_x) \\ &= 9.17\ \text{Å}\ b_{est} = 9.00\ \text{Å}\ \alpha = 11°, \\ P_I = 0.95&: b_{oct} = 8.14\ \text{Å}\ b(Si_{1-x}Al_x) \\ &= 9.28\ \text{Å}\ b_{est} = 9.00\ \text{Å}\ \alpha = 14°. \end{aligned} \quad (2)$$

The diagenetic cation substitutions in the octahedral sheet amounted to only ⅓ (calculated from Figure 8) of the octahedral cations and only ⅓ of these (Al^{3+}-for-Mg^{2+} or -Fe^{2+} substitutions) influenced octahedral sheet dimensions. Thus, altogether the octahedral sheet dimensions decreased slightly during diagenesis. The constant d(060) during tetrahedral Al-for-Si substitution can be explained by an increased tetrahedral rotation from 11° to 14°.

Correspondence between XRD and NMR

The linear correlation shown in Figure 8B gives an increase of 0.28 $Al^{IV}/(Si + Al^{IV})$ per 1.0 P_I, i.e., of 1.1 Al^{IV} for formation of a pure illite from a pure smectite. This is in good agreement with the difference between the end members of the mica-smectite series (Bailey, 1984). The lines in Figure 8A and 8B, however, have zero Al^{IV} at P_I values of 0.37 and 0.39, respectively. A value of Al^{IV} of 0.69 per $O_{10}(OH)_2$ at a P_I value of 1.0 is calculated from the plot in Figure 8B. The value of 0.69 for Al^{IV} at $P_I = 1.0$, an octahedral charge of about −0.2 originating from substitution by Mg^{2+} and Fe^{2+}, and a total charge of −0.9 are all in agreement with the illite data of Hower and Mowatt (1966). If the lines of the plots for % MgO and % Fe_2O_3 vs. P_I in Figures 7D–7E are extended to intercept with the horizontal axis, the intercepts are at $P_I = 1.3$ for both lines. Recently, Altaner *et al.* (1988) found that the fraction of illite layers in I/S calculated from ^{29}Si NMR is significantly lower than the fraction calculated from XRD. This is in agreement with the present NMR and XRD results for which the NMR spectra show a significantly higher Al^{IV} content in smectite layers than should be expected from the XRD results. According to the plots of % MgO, % Fe_2O_3, Al^{IV}/Al^{VI}, and $Al^{IV}/(Al^{VI} + Si)$ vs. P_I, the values for these compositional parameters at $P_I = 0$ and $P_I = 1$ will be those of the ideal end members of the smectite-mica series, if the P_I values from XRD are assumed to be about 0.35 too high. According to this assumption, R1 ordering will take place at a corrected P_I value of 0.8–0.35, i.e., at about 0.5 which is the ideal value for this ordering. This supports the conclusion from combined NMR and XRD data, i.e., illite layers differ from pure mica in having smectite sites.

Charges of illite and smectite layers

Eberl (1986) reported thermodynamical calculations on the K^+ for Na^+ ion exchange during smectite diagenesis, assuming that illite layers formed by a solid-state transformation. He concluded that a cation in a smectite interlayer dehydrates in response to increasing interlayer charge and that, for the same charge, the smallest ion is fixed preferentially. The ionic radii for dehydrated NH_4^+, K^+, and Na^+ are 1.43, 1.33, and 0.98 Å, respectively (Sterne *et al.*, 1982; Eberl, 1986). Therefore, if these ions are hydrated, $Na(aq.)^+$ has the largest radius and $NH_4(aq.)^+$ the smallest, and $Na(aq.)^+$ requires the largest and $NH_4(aq.)^+$ the smallest interlayer charge for dehydration. Application of the principles of Eberl (1986) to the NH_4^+-K^+-Na^+ ion exchange and fixation during smectite diagenesis therefore results in the following sequence: at low smectite interlayer charge all cations are hydrated and $NH_4(aq.)^+$ is sorbed with slight preference to $K(aq.)^+$, and $K(aq.)^+$ is sorbed with slight preference to $Na(aq.)^+$. With increasing interlayer charge, $NH_4(aq.)^+$ is first dehydrated and then fixed highly preferentially to $K(aq.)^+$ and $Na(aq.)^+$. With a further small increase in interlayer charge, $K(aq.)^+$ is also dehydrated and then fixed slightly preferentially to NH_4^+, but highly preferentially to $Na(aq.)^+$. The increasing amount of NH_4^+ at about $P_I = 0.7$ (Figure 7A) may thus be explained from a preferential fixation of dehydrated NH_4^+ compared to $K(aq.)^+$ and $Na(aq.)^+$ at this P_I level.

For each illite layer formed (corresponding to an increase in P_I with 1.0) the total amount of interlayer cations increase with 0.4 (Figure 7H) equivalents, the negative octahedral charge decreases with 0.55 (calculated from the decrease in divalent, octahedral cations from Figures 7D and E and Table 5), and the negative tetrahedral charge increases with 1.1, all per $O_{10}(OH)_2$ (Figure 8B). A contribution to the increase in octahedral charge through Fe^{3+} reduction is not apparent in the present investigation. The octahedral charge reduction and the tetrahedral charge increase are due to Al^{3+} substitution, in the tetrahedral sheet for Si^{4+} and in the octahedral sheet for Mg^{2+} and Fe (mainly Fe^{3+}). About ⅔ of the increase in octahedral Al occurs through substitution for Fe^{3+}, which does not decrease the layer charge. The net increase in negative charge of the 2:1 unit is 1.1–0.55, i.e., 0.55, which

https://doi.org/10.1346/CCMN.1991.0390108 Published online by Cambridge University Press

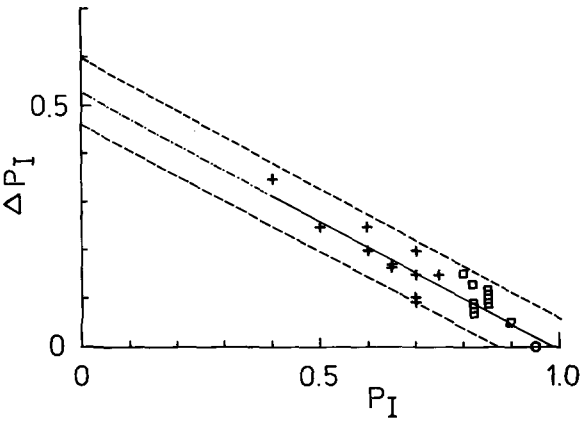


Figure 9. ΔP_I (increase in P_I for glycolated illite/smectite specimens obtained by exchange of Mg^{2+} with K^+) vs. P_I for Mg^{2+}-saturated specimens; correlation coefficient of −0.91. Solid line is regression line; dotted lines delimit two standard deviations. Symbols: + = R0-ordered; □ = R1-ordered; ○ = R3-ordered illite/smectite.

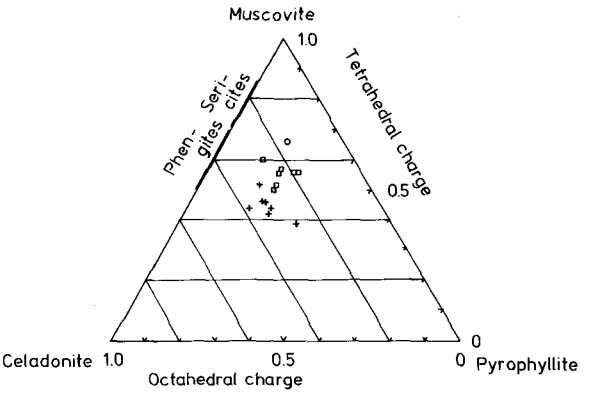


Figure 10. Triangular plot for calculated illite/smectite formulae.

corresponds reasonably well with the increase in interlayer cations of 0.4. Thus, the fixation of 0.75 mole $NH_4^+ + K^+$ per $O_{10}(OH)_2$ is caused by a net charge increase of 0.55 and a migration of a charge of 0.55 from the octahedral to the tetrahedral sheet. This migration causes the charge to interact with the interlayer cations with stronger coulombic forces and therefore makes fixation possible. The predominantly tetrahedral increase in charge with P_I is in agreement with previous results (Foscolos *et al.*, 1976; Eberl and Hower, 1976; Eslinger *et al.*, 1979; Hower, 1981).

Between 0 and 35% of the layers found to be smectite in the Mg^{2+}-saturated and glycolated specimens fail to expand with ethylene glycol after K^+-saturation (Table 1). Walker (1961) found that K^+-saturated high-charge smectites fail to expand with ethylene glycol, in the same manner as vermiculites. Therefore, about half of the smectite layers in Mg^{2+}-saturated and glycolated or air-dry specimens must possess a high charge. The remaining smectite layers must also possess a significant charge, as only one interlayer of glycol forms in K^+-saturated specimens. The fraction of layers that are smectitic in Mg^{2+}-saturated specimens but which do not expand with glycol after K^+-saturation is called ΔP_I. In Figure 9 ΔP_I is plotted vs. P_I, as determined for Mg^{2+}-saturated specimens. The amount of high-charge smectite layers (ΔP_I) decreases linearly with increasing P_I. An increase in P_I by one unit yields $\Delta P_I = 0.53$. Thus, diagenetic formation of one illite layer is accompanied by disappearance of half a high-charge smectite layer. In each sample, irrespective of P_I, about half the smectite layers are high charge and the other half low charge. This indicates that the illite layers are not formed by dissolution of either low- or high-charge smectite layers. The observation can be explained, however, by a solid-state Al-for-Si substitution in all smectite layers, whereby high-charge layers become illitic and half of the low-charge layers become high-charge. The observation can also be explained from a random dissolution of smectite layers irrespective of charge.

Hower and Mowatt (1966) plotted the elementary compositions of mixed layers of illite and montmorillonite in a ternary celadonite-muscovite-pyrophyllite diagram. They found that the contours for the percentage of expandable layers were parallel to the mica side. Thus, the percentage of expandable layers apparently are not affected by tetrahedral-octahedral charge distributions, but only by the total charge. The I/S samples of the present investigation are plotted similarly in Figure 10. The contours for ordering of the I/S in Figure 10 are parallel to the pyrophyllite-celadonite side. Thus, the ordering results from increasing tetrahedral charge through Al-for-Si substitution, a result that is also suggested by the high degree of correlation between Al(4)/[Al(4) + Si] and P_I in Figure 8B.

Reaction pathways for formation of illite from smectite layers

The two different models proposed for the formation of illite layers from smectite layers have structural implications for the illite and smectite layers in rocks. In the transformation model, illite is formed from smectite through a solid-state Al^{3+}-for-Si^{4+} substitution and a subsequent K^+ fixation between 2:1 units. This results in smectite layers having varying amounts of tetrahedral substitution. In the neoformation model, illite layers crystallize and grow from a solution. This yields neoformed illite crystals with the same substitution in all illite layers and indicates that the top and bottom tetrahedral sheets in the illite crystals have an illitic degree of Al-for-Si substitution.

The results on the Upper Jurassic I/S conform with those of Altaner *et al.* (1988) in the finding of smectitic sites in so large of amounts that they must be present in 2:1 units, which, according to XRD, are illitic. Ac-

https://doi.org/10.1346/CCMN.1991.0390108 Published online by Cambridge University Press

cording to ^{29}Si NMR, the increase in tetrahedral Al results exclusively in Si(1Al) sites (Figure 11A), whereas the number of Si(2Al) sites appears to be constant in the P_I interval investigated (Figure 11B). This shows that the Al-for-Si substitution during illite formation is ordered, in agreement with the finding of Besson *et al.* (1974) that tetrahedral substitution in illites and partly in vermiculites is ordered.

The presence of smectitic sites in illite layers and illitic sites in the smectite layers show that the illite layers have been formed by a transformation and not by a neoformation from smectite layers. A transformation mechanism can explain the constant ratio between high- and low-charge smectite layers irrespective of degree of diagenesis. It also explains the increased fixation of NH_4^+ at $P_I = 0.7$ as described above. The solid-state Al^{3+} substitution, however, occurs both in the tetrahedral sheets for Si^{4+} and in the octahedral sheets for Mg^{2+}, Fe^{2+}, and Fe^{3+} during the formation of illite layers from smectite layers.

The presence of illite and smectite layers, each with their specific tetrahedral and octahedral substitution pattern as implicated in the neoformation model by Nadeau *et al.*, (1985) should result in two distinct 060 reflections. The observed sharpening of the 060 reflection with increasing P_I agrees better with the transformation model. According to this model, different degrees of substitution in illite and smectite layers produces more uniformly substituted illite layers at high P_I-values. As a result, the 060 reflection should become sharper, as has been observed.

The solid-state transformation was previously proposed for I/S in shales and bentonites by Hower *et al.* (1976). The neoformation mechanism was proposed by Nadeau *et al.* (1985), who investigated diagenetic illitic clays from sandstones and bentonites. The neoformation mechanism for sandstone illitic clays has been well documented by scanning electron microscopy (Nadeau *et al.*, 1985). It also appears a likely mechanism for bentonitic parent material, in which smectite must form by dissolution of the volcanic glass.

In the present investigation, however, the formation of illite layers from smectite layers during burial diagenesis in the Upper Jurassic claystones most likely was a solid-state transformation. The mechanism for illite layer formation may therefore be different depending on the type of parent material (sandstones, bentonite, or claystone) and diagenesis (burial diagenesis, hydrothermal transformation, or low-grade metamorphism). The amount of smectite layers in the I/S parent material can be a determining factor. Thus, conversion of a pure smectite to I/S containing 85% illite layers requires six times the Al compared with the Al required for conversion of the North Sea parent material containing 70% illite layers in I/S (assuming a similar percentage of I/S in the bulk rock). Therefore, a dissolution of smectite layers may be necessary for pure smectite parent material, whereas a solid-state transformation is possible for the I/S of the North Sea.

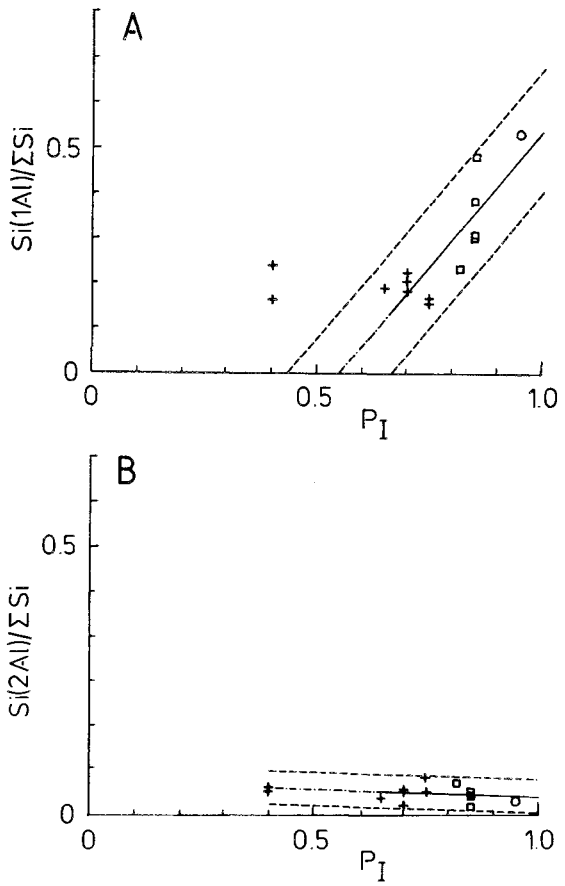


Figure 11. A = Si(1Al)/ΣSi ratios of illite/smectite (I/S) samples (calculated from ^{29}Si nuclear magnetic resonance (NMR) spectroscopy) vs. P_I; correlation coefficient of 0.85. B = Si(2Al)/Σ Si ratios of I/S calculated from ^{29}Si NMR) vs. P_I; correlation coefficient of 0.17. The two points at 0.4 are omitted from the regression analysis.

ACKNOWLEDGMENTS

The investigation was financially supported by the Danish Natural Science Research Council (SNF) (J.no. 11-5556) and was carried out while H. Lindgreen occupied a senior research fellowship at the University of Copenhagen. The Norwegian samples were provided by the Norwegian Petroleum Directorate and the Danish samples by the Geological Survey of Denmark. The use of the facilities at the University of Aarhus NMR Laboratory, sponsored by the Danish Research Councils (SNF and STVF), Carlsbergfondet, and Direktør Ib Henriksens Fond, is acknowledged.

REFERENCES

Altaner, S. P., Weiss, S. A., and Kirkpatrick, R. J. (1988) Evidence from ^{29}Si NMR for the structure of mixed-layer illite/smectite clay minerals: *Nature* **331,** 699–702.

https://doi.org/10.1346/CCMN.1991.0390108 Published online by Cambridge University Press

Anderson, J. U. (1963) An improved pretreatment for mineralogical analysis of samples containing organic matter: in *Clays and Clay Minerals, Proc. 10th Natl. Conf., Austin, Texas, 1961,* A. Swineford and P. C. Franks, eds., Pergamon Press, New York, 380–388.

Bailey, S. W. (1984) Structures of layer silicates: in *Crystal Structures of Clay Minerals and Their X-ray Identification,* G. W. Brindley and G. Brown, eds., Mineralogical Society, London, 1–124.

Barnard, P. C. and Cooper, B. S. (1981) Oils and source rocks of the North Sea area: in *Petroleum Geology of the Continental Shelf of North-West Europe,* L. V. Illing and G. D. Hobson, eds., Heyden and Son, London, 169–175.

Bernas, B. (1968) A new method for decomposition and comprehensive analysis of silicates by atomic absorption spectroscopy: *Anal. Chem.* **40,** 1682–1686.

Besson, G., Mifsud, A., Tchoubar, C., and Méring, J. (1974) Order and disorder relations in the distribution of the substitutions in smectites, illites, and vermiculites: *Clays & Clay Minerals* **22,** 379–384.

Bethke, C. M. and Reynolds, R. C. (1986) Recursive method for determining frequency factors in interstratified clay diffraction calculations: *Clays & Clay Minerals* **34,** 224–226.

Buzagh, A. and Szepesi, K. (1955) A colloid-chemical method for the determination of the montmorillonite content in bentonites: *Acta Chim. Hung.* **5,** 287–298.

Cardile, C. M. (1987) Structural studies of montmorillonites by ^{57}Fe Mössbauer spectroscopy: *Clay Miner.* **22,** 387–394.

Cradwick, P. D. and Wilson, M. J. (1978) Calculated X-ray diffraction curves for the interpretation of a three-component interstratified system: *Clay Miner.* **13,** 53–65.

Deer, W. A., Howie, R. A., and Zussman, J. (1967) *Rock Forming Minerals, Vol. 3, Sheet Silicates:* Longmans, London, 270 pp.

Dunoyer de Segonzac, G. (1970) The transformation of clay minerals during diagenesis and low-grade metamorphism: A review: *Sedimentology* **15,** 281–346.

Eberl, D. D. (1976) Reaction series for dioctahedral smectites: *Clays & Clay Minerals* **26,** 327–340.

Eberl, D. D. (1986) Sodium-potassium ion exchange during smectite diagenesis—A theoretical discussion: in *Studies in Diagenesis,* F. A. Mumpton, ed., *U.S. Geol. Surv. Bull.* **1578,** 363–368.

Eberl, D. D. and Hower, J. (1976) Kinetics of illite formation: *Geol. Soc. Amer. Bull.* **87,** 1326–1330.

Eslinger, E., Highsmith, P., Albers, D., and DeMayo, B. (1979) Role of iron reduction in the conversion of smectite to illite in bentonites in the Disturbed Belt, Montana: *Clays & Clay Minerals* **27,** 327–338.

Foscolos, A. E. and Powell, T. G. (1979) Mineralogical and geochemical transformations of clays during burial-diagenesis (catagenesis): Relation to oil generation: in *Proc. Int. Clay Conf., Oxford, 1978,* M. M. Mortland and V. C. Farmer, eds., Elsevier, Amsterdam, 261–270.

Foscolos, A. E., Powell, T. G., and Gunther, P. R. (1976) The use of clay minerals and inorganic and organic geochemical indicators for evaluating the degree of diagenesis and oil potential of shales: *Geochim. Cosmochim. Acta* **40,** 953–966.

Frank-Kamenetskii, V. A., Kotelnikova, E. N., Kotov, N. V., and Starke, S. (1979) Influence of tetrahedral aluminum on the hydrothermal transformation of montmorillonite and beidellite to mixed-layer illite-montmorillonite and illite: *Kristall und Technik* **14,** 303–314.

Frye, J. S. and Maciel, G. E. (1982) Setting the magic angle using a quadrupolar nucleide: *J. Magn. Res.* **48,** 125–131.

Gibbs, R. J. (1967) Quantitative X-ray diffraction analysis using clay mineral standards extracted from the samples to be analysed: *Clay Miner.* **7,** 79–90.

Goodman, B. A. (1976) The Mössbauer spectrum of a ferrian muscovite and its implications in the assignment of sites in dioctahedral micas: *Mineral. Mag.* **40,** 513–517.

Goodman, B. A. (1987) On the use of Mössbauer spectroscopy for determining the distribution of iron in aluminosilicate minerals: *Clay Miner.* **22,** 363–366.

Goodman, B. A. and Stucki, J. W. (1984) The use of nuclear magnetic resonance (NMR) for the determination of tetrahedral aluminum in montmorillonite: *Clay Miner.* **19,** 663–667.

Guggenheim, S. and Eggleton, R. A. (1987) Modulated 2:1 layer silicates: Review, systematics, and predictions: *Amer. Mineral.* **72,** 724–738.

Hansen, P. L. and Lindgreen, H. (1989) Mixed-layer illite/smectite diagenesis in Upper Jurassic claystones from the North Sea and onshore Denmark: *Clay Miner.* **24,** 197–213.

Higashi, S. (1978) Dioctahedral mica minerals with ammonium ions: *Mineral. J.* **9,** 16–27.

Howard, J. J. (1981) Lithium and potassium saturation of illite/smectite clays from interlaminated shales and sandstones: *Clays & Clay Minerals* **29,** 136–142.

Hower, J. (1981) Shale diagenesis: in *Clays and the Resource Geologist,* F. J. Longstaffe, ed., Mineral. Assoc. Canada, 40–60.

Hower, J., Eslinger, E. V., Hower, M. E., and Perry, E. A. (1976) Mechanisms of burial metamorphism of argillaceous sediment: 1. Mineralogical and chemical evidence: *Bull. Geol. Soc. Amer.* **87,** 725–737.

Hower, J. and Mowatt, T. C. (1966) The mineralogy of illites and mixed-layer illite/montmorillonites: *Amer. Mineral.* **51,** 825–854.

Jakobsen, H. J., Daugaard, P., and Langer, V. (1988a) CP/MAS NMR at high speeds and high fields: *J. Magn. Res.* **76,** 162–168.

Jakobsen, H. J., Jacobsen, H., and Lindgreen, H. (1988b) Solid state ^{27}Al and ^{29}Si MAS n. m. r. studies on diagenesis of mixed-layer silicates in oil source rocks: *Fuel* **67,** 727–730.

Jensen, E. and Hansen, H. M. (1961) An elutriator for particle-size fractionation in the sub-sieve range: *Soil Sci.* **92,** 94–99.

Johnston, J. H. and Cardile, C. M. (1985) Iron sites in nontronite and the effect of interlayer cations from Mössbauer spectra: *Clays & Clay Minerals* **33,** 21–30.

Kinsey, R. A., Kirkpatrick, R. J., Hower, J., Smith, K. A., and Oldfield, E. (1985) High resolution aluminium-27 and silicon-29 nuclear magnetic resonance spectroscopy study of layer silicates, including clay minerals: *Amer. Mineral.* **70,** 537–548.

Komarnemi, S., Fyfe, C. A., Kennedy, G. J., and Strobl, H. (1986) Characterization of synthetic and naturally occurring clays by ^{27}Al and ^{29}Si magic-angle spinning NMR spectroscopy: *J. Amer. Ceram. Soc.* **69,** C45–C47.

Middelboe, V. (1977) Determination of trace amounts of total nitrogen by isotope dilution: in *Stable Isotopes in the Life Sciences, Proc. Technical Committee Meeting on Biological Applications of Stable Isotopes, Leipzig, 1977,* International Atomic Agency, Council for Mutual Economic Assistance, 239–243.

Nadeau, P. H., Wilson, M. J., McHardy, W. J., and Tait, J. M. (1985) The conversion of smectite to illite during diagenesis: Evidence from some illitic clays from bentonites and sandstones: *Mineral. Mag.* **49,** 393–400.

Perry, E. and Hower, J. (1972) Late-stage dehydration in deeply buried pelitic sediments: *Amer. Assoc. Pet. Geol. Bull.* **56,** 2013–2021.

Powers, M. C. (1959) Adjustment of clays to chemical change and the concept of the equivalence level: in *Clays and Clay*

https://doi.org/10.1346/CCMN.1991.0390108 Published online by Cambridge University Press

Minerals, Proc. 6th Natl. Conf, Austin, Texas, 1961, A. Swineford and P. C. Franks, eds., Pergamon Press, New York, 380–388.

Radoslovich, E. W. (1961) Surface symmetry and cell dimensions of layer-lattice silicates: *Nature* **191,** 67–68.

Reynolds, R. C. (1984) Interstratified clay minerals: in *Crystal Structures of Clay Minerals and Their X-ray Identification,* G. W. Brindley and G. Brown, eds., Mineralogical Society, London, 249–304.

Roth, C. B., Jackson, M. L., and Syers, J. K. (1969) Deferration effect on structural ferrous-ferric iron ratio and CEC of vermiculites and soils: *Clays & Clay Minerals* **17,** 253–264.

Samoson, A. (1985) Satellite transition high-resolution NMR of quadrupolar nuclei in powders: *Chem. Phys. Lett.* **119,** 29–32.

Środoń, J., Morgan, D. J., Eslinger, E. V., Eberl, D. D., and Karlinger, M. R. (1986) Chemistry of illite/smectite and end-member illite: *Clays & Clay Minerals* **34,** 368–378.

Sterne, E. J., Reynolds, R. C., and Zantop, H. (1982) Natural ammonium illites from black shales hosting a stratiform base metal deposit, Delong Mountains, northern Alaska: *Clays & Clay Minerals* **30,** 161–166.

Thomas, J. M. and Klinowski, J. (1985) The study of aluminosilicates and related catalysts by high-resolution solid-state NMR spectroscopy: *Adv. Catalysis* **33,** 199–396.

Thompson, J. G. (1984) ^{29}Si and ^{27}Al nuclear magnetic resonance spectroscopy of 2:1 clay minerals: *Clay Miner.* **19,** 229–236.

Velde, B. and Brusewitz, A. M. (1986) Compositional variation in component layer in natural illite/smectite: *Clays & Clay Minerals* **34,** 651–657.

Walker, G. G. (1961) Vermiculite minerals: in *X-ray Identification and Crystal Structures of Clay Minerals,* G. Brown, ed., Mineralogical Society, London, 297–324.

Weiss, C. A., Altaner, S. P., and Kirkpatrick, R. J. (1987) High resolution ^{29}Si NMR spectroscopy of 2:1 layers: Correlations among chemical shift, structural distortions and chemical variations: *Amer. Mineral.* **72,** 935–942.

(Received 24 April 1989; accepted 9 August 1990; Ms. 1908)

https://doi.org/10.1346/CCMN.1991.0390108 Published online by Cambridge University Press